Journal of Micromechanics and Microengineering

PAPER

Molybdenum disulfide dc contact MEMS shunt switch

To cite this article: Peng Li *et al* 2013 *J. Micromech. Microeng.* **23** 045026

J. Micromech. Microeng. **23** (2013) 045026 (6pp) doi:10.1088/0960-1317/23/4/045026

Molybdenum disulfide dc contact MEMS shunt switch

Peng Li[1,2], **Zheng You**[1] **and Tianhong Cui**[1,2]

[1] State Key Laboratory of Precision Measurement Technology and Instruments, Department of Precision Instruments and Mechanology, Tsinghua University, Beijing 100084, People's Republic of China
[2] Department of Mechanical Engineering, University of Minnesota, Minneapolis, MN 55455, USA

E-mail: tcui@me.umn.edu and yz-dpi@mail.tsinghua.edu.cn

Received 7 December 2012, in final form 15 February 2013
Published 19 March 2013
Online at stacks.iop.org/JMM/23/045026

Abstract
Atomic force microscopy pulsed force mode verifies that molybdenum disulfide (MoS_2) has a smaller surface adhesion energy than graphene. MEMS switches based on MoS_2 may have less stiction problems. Suspended MoS_2 two-end fixed beams were fabricated, and their mechanical properties including Young's modulus were characterized by atomic force microscope (AFM) indentation. MoS_2 dc contact MEMS (micro-electro-mechanical systems) switches were demonstrated with a pull-in voltage of less than 10 V.

S Online supplementary data available from stacks.iop.org/JMM/23/045026/mmedia

(Some figures may appear in colour only in the online journal)

1. Introduction

A switch is an important MEMS device. Compared with a field effect transistor, the 'off-state' current of MEMS dc switches is 0 [1–3], and MEMS RF switches have better isolation [4–6]. Although some of the MEMS switches have been commercialized, there are still challenges for broader applications [7, 8]. Many researchers focus on using new materials, including two-dimensional materials, to fabricate MEMS switches for better performance. To date the most widely investigated 2D material is graphene [9, 10] because it has high carrier mobility [11] and Young's modulus [12–14]. However, a graphene membrane has a very strong adhesion force [15–19]. Therefore, MEMS switches based on graphene may encounter stiction problems [2, 20–22]. An MoS_2 crystal is composed of vertically stacked layers bonded together by the van der Waals force. Single layer MoS_2 is only 0.65 nm thick, and can be obtained by mechanical exfoliation [23] and chemical vapor deposition [24]. Radisavljevic *et al* took advantage of the unique electrical properties of MoS_2, and fabricated the first MoS_2 transistor with an on/off ratio over 1×10^8 [25]. Single/few-layer MoS_2 also has excellent mechanical properties. Its Young's modulus is about 200–300 GPa [26–28]. In this paper we investigate the mechanical properties of MoS_2, and demonstrate the first MEMS switch based on MoS_2.

2. Experiment, results and discussion

2.1. Comparison of MoS_2 and graphene

A few-layer sample of MoS_2 was exfoliated from MoS_2 crystals using a mechanical exfoliation method (see supplementary information (available at stacks.iop.org/JMM/23/045026/mmedia)). The adhesion energy of the material can be measured by AFM indentation [29–31]. Using an AFM pulsed force mode (PFM) (see supplementary information (available at stacks.iop.org/JMM/23/045026/mmedia)), we compared MoS_2 and graphene flakes transferred onto a Si/SiO_2 substrate. In the MEMS region, the adhesion energy between Si (SiO_2) and the target material has a large influence on the performance of the devices. Therefore, we chose the Si AFM tip coated by a layer of SiO_2. Figures 1(*a*) and (*c*) are AFM topographical images, and figures 1(*b*) and (*d*) are corresponding adhesion force images (they are 1024×1024 pixels derived from the same AFM tip, and the brighter color indicates a stronger adhesion force between the AFM tip and the sample surface). To diminish the impact of the capillary force, we purged the chamber with nitrogen during the experiment, keeping the humidity value between 2% and 5%. Figure 1(*d*) demonstrates that the colors of the MoS_2 and SiO_2 substrate do not have obvious differences (they have

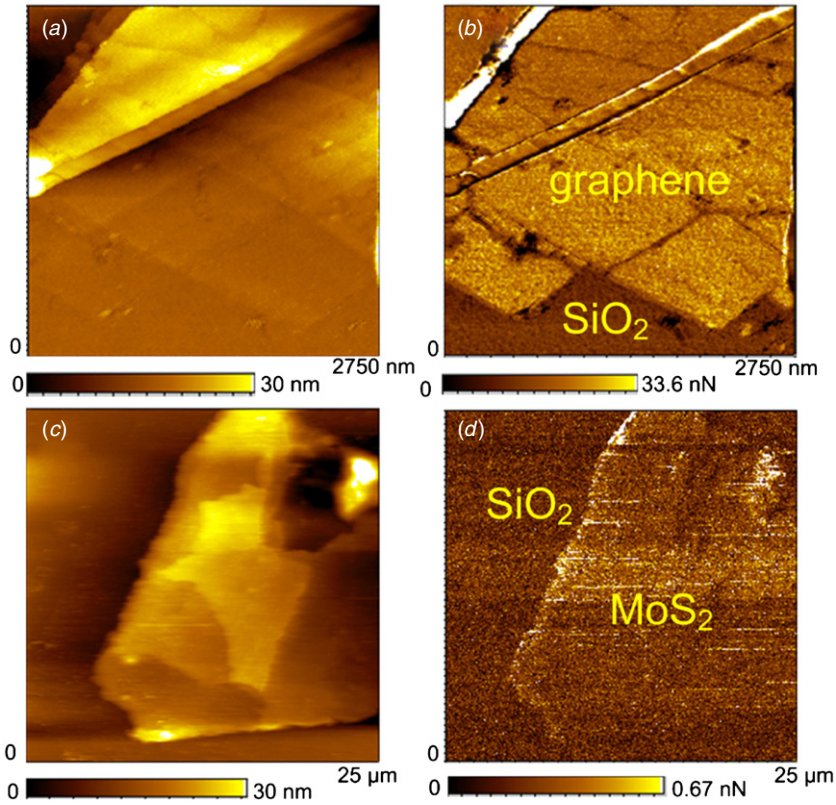

Figure 1. Comparison of the adhesion force of graphene and MoS_2. (*a*) AFM topographical image of graphene on a SiO_2 substrate. (*b*) Corresponding AFM adhesion force image of graphene on a SiO_2 substrate. (*c*) Topographical image of MoS_2 on a SiO_2 substrate. (*d*) Corresponding adhesion force image of MoS_2 on a SiO_2 substrate.

a similar adhesion force). According to the Maugis model [32], the adhesion force is in proportion to the adhesion energy per unit of area between two materials. Therefore, the MoS_2/SiO_2 (tip) adhesion energy is similar to the SiO_2/SiO_2 (tip) adhesion energy. In figure 1(*b*) the colors of the graphene and SiO_2 substrate have obvious differences, indicating that the graphene/SiO_2 adhesion energy is larger than that of SiO_2/SiO_2. By comparing figures 1(*b*) and (*d*), we know that graphene's surface is much 'stickier' than MoS_2. Compared with graphene, when the MoS_2 switch is set to a down position, it has less chance to encounter a stiction problem.

2.2. *Fabrication of a suspended MoS_2 beam*

The fabrication process of suspended beam structures, as shown in figure 2, starts with depositing Cr/Au/Ti (10 nm/100 nm/10 nm) by electron-beam evaporation on top of a Si substrate. Cr and Ti work as the bottom and top adhesion layers, respectively. Ti can be removed together with S_iO_2 by a wet etching process using buffered oxide etchant (BOE). Therefore, MoS_2 beams can be electrically in contact with the Au layer with a good conductivity. Sequentially, SiO_2 300 nm thick was deposited on top of metal layers by plasma enhanced chemical vapor deposition as an isolation layer. Next, we used a mechanical exfoliation method to transfer MoS_2 on top of the SiO_2. The sequential fabrication of electrodes involves photolithography, Cr/Au electron-beam evaporation and metal

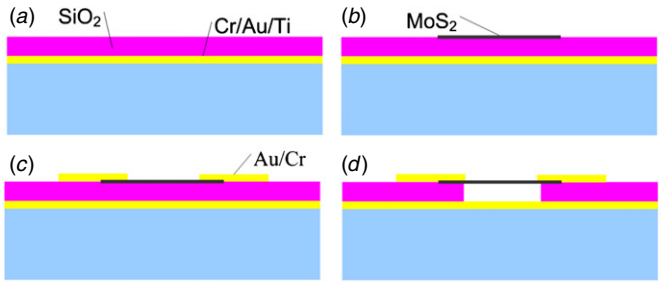

Figure 2. Fabrication process of suspended MoS_2 structures. (*a*) Deposit Cr/Au/Ti on top of a Si substrate. PECVD is used to grow SiO_2 300 nm thick on top of metal layers. (*b*) Transfer mechanically exfoliated a few-layer MoS_2 flakes onto a SiO_2/Si substrate. (*c*) Photolithography and image reversal technique were used to define the electrodes. Electrodes were fabricated by Cr/A_u (10 nm/100 nm) deposition and lift-off process. (*d*) BOE was used to etch SiO_2 and Ti beneath MoS_2, followed by critical point drying.

lift-off. The samples were rinsed in BOE for 4 min to etch the SiO_2 and Ti layers beneath the MoS_2, followed by a critical point drying which can keep the structures suspended during wet etching. The success rate of MoS_2 devices fabrication is over 90%. The failure usually happened during the BOE wet etching and the critical point drying process. Figure 3(*a*) shows the SEM image of a free-standing MoS_2 beam which is clearly wrinkled because of the pretension of the fabrication.

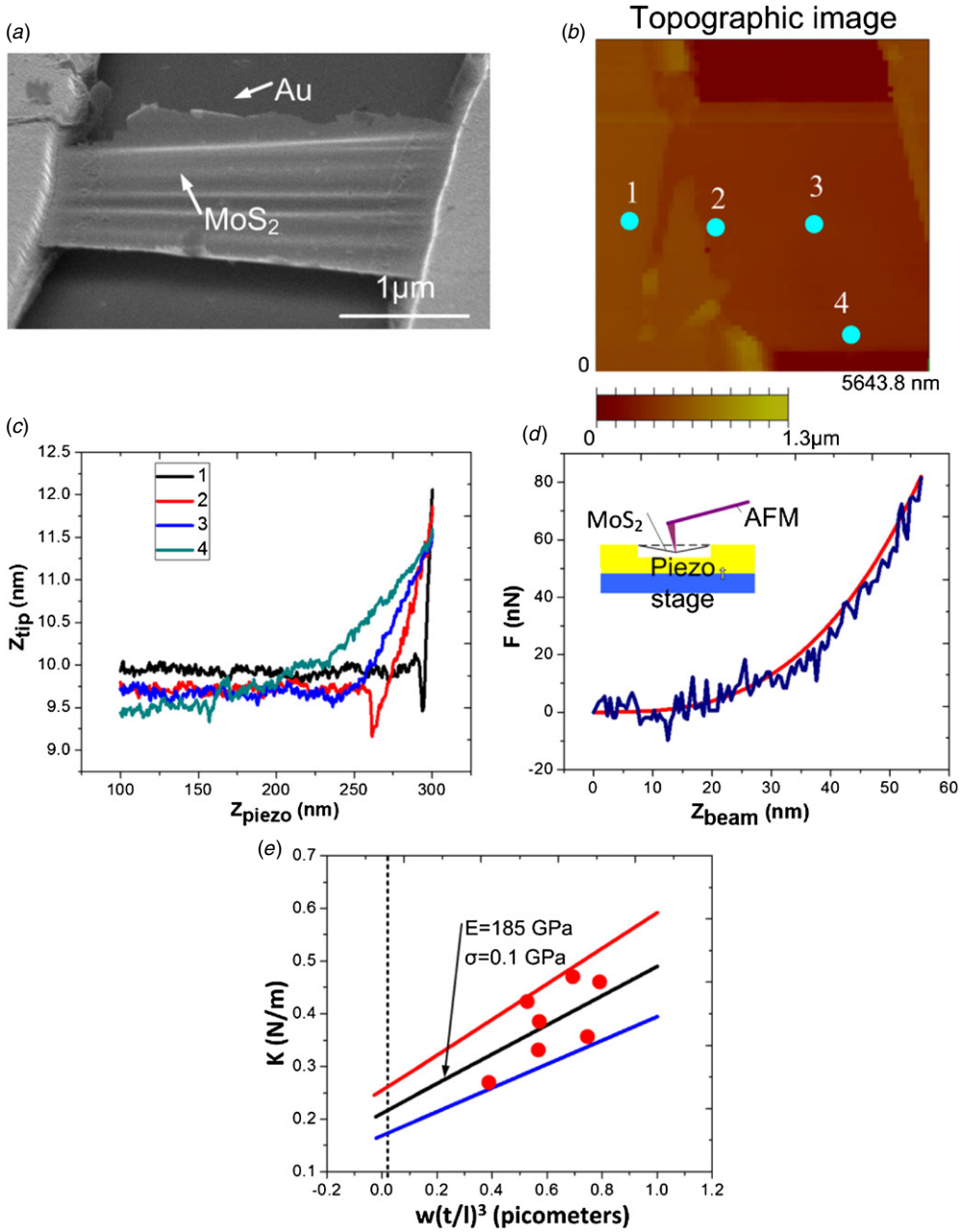

Figure 3. Mechanical properties of a few-layer MoS_2 characterized by AFM indentation. (*a*) SEM image of a suspended MoS_2 beam. (*b*) AFM topographical image of a suspended MoS_2. (c) Z_{piezo} versus Z_{tip} curve of 4 spots indicated in figure 3(*b*). (*d*) Force versus displacement curve of a MoS_2 beam. The red line indicates the force curve is in proportion to Z^3_{beam} in large deflection region. (*e*) A plot of the spring constant of the MoS_2 sheets, versus $w(t/L)^3$ for seven different samples. The Young's modulus and pretension could be extracted from the linear fit.

Graphene can be etched by O_2 plasma quickly [33]. Therefore, graphene devices cannot be exposed to O_2 plasma to completely remove the residues. They have to be annealed instead. Nevertheless, not all of the device can stand such high temperatures. We treated the MoS_2 and graphene samples with O_2 plasma dry etching to completely remove the photoresist residuals and other contaminants after fabrication. After 1 min dry etching the MoS_2 layer had no obvious change, while the graphene layers were etched away completely. Therefore, MoS_2-based devices can be easily cleaned by O_2 plasma.

2.3. Investigation of the mechanical properties of an MoS_2 beam

Mechanical properties of few-layer MoS_2 beams were investigated by an AFM. We calibrated the AFM cantilever before imaging. The spring constant of the cantilever, Z_{tip}, was 1.2 N m^{-1} (see supplementary information (available at stacks.iop.org/JMM/23/045026/mmedia)). A multimodal AFM was used to acquire topographic images of a free-standing MoS_2 beam (figure 3(*b*)), and to collect force-*Z* curves (see supplementary information (available at stacks.iop.org/JMM/23/045026/mmedia)) in a location of

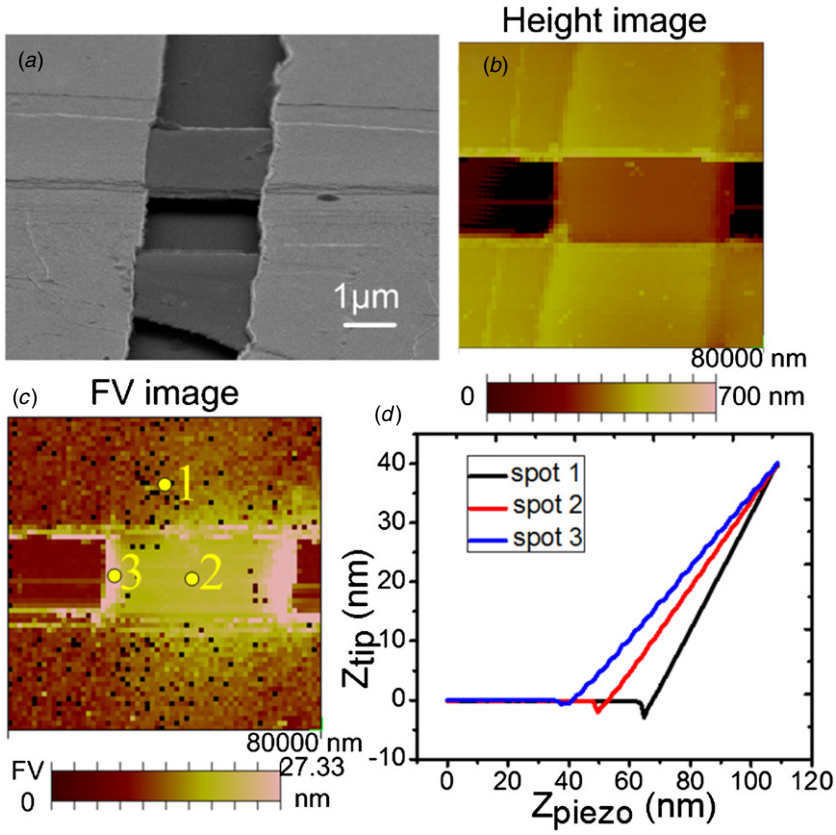

Figure 4. Mechanical properties of thick MoS_2 characterized by AFM indentation. (*a*) SEM image of two suspended thick MoS_2 beams. (*b*) AFM topographical image of a thick MoS_2 beam. (*c*) AFM force volume image of the same suspended beam. (*d*) Z_{piezo} versus Z_{tip} curve of three spots indicated in figure 4(*c*).

64 × 64 grids (also called the 'force volume') for mechanical assessment. During indentation, the MoS_2 beam was bent, and the force against the sheet also caused the AFM cantilever to deflect. The relationship among the MoS_2 beam's displacement, Z_{beam}, the piezo stage movement beneath the sample, Z_{piezo}, and the AFM cantilever deflection, Z_{tip}, is:

$$Z_{beam} = Z_{piezo} - Z_{tip}. \tag{1}$$

The force, F, applied to the MoS_2 beam can be derived by:

$$F = K_{tip} Z_{tip}. \tag{2}$$

The force-Z data cube provides a 2D mapping of local stiffness. It provides us with sufficient information about the stiffness distribution. The force curves in figure 3(*c*) are derived from the four different spots indicated in figure 3(*b*). They do not only demonstrate the distribution of the stiffness on the beam, but also imply that a few-layer MoS_2 beam (2.5 nm in thickness) is a nonlinear system. The double clamped beam model [2, 13, 14, 34, 35] can provide a good approximation for our case. In a pure bending regime, the relationship between force and center displacement of a double clamped beam under a concentrated force is given by [34, 36]:

$$\begin{aligned} F &= k_{bending} Z_{beam} + k_{stress} Z_{beam} + k_{stretching} Z_{beam}^3 \\ &= \frac{E w \pi^4}{6}\left(\frac{t}{l}\right)^3 Z_{beam} + \frac{w \sigma \pi^2}{2}\left(\frac{t}{l}\right) Z_{beam} \\ &\quad + \frac{E w \pi^4}{8}\left(\frac{t}{l^3}\right) Z_{beam}^3 \end{aligned} \tag{3}$$

where E is the MoS_2 Young's modulus, σ is the initial stress in the beam, and l, w and t are the length, width and thickness of the beam, respectively. For a few-layer MoS_2 beam with a large deformation, the stretching term is in dominant, and the red line in figure 3(*d*) demonstrates that F is proportional to Z^3_{beam} in the large deflection region. In the limit of a small deformation, the spring constant of the beam is:

$$k = \frac{\partial F}{\partial Z_{beam}} \approx \frac{E w \pi^4}{6}\left(\frac{t}{l}\right)^3 + \frac{w \sigma \pi^2}{2}\left(\frac{t}{l}\right). \tag{4}$$

For all the beams we measured, the $w(t/l)^3$ term is expected to vary much more than the $\sigma w(t/l)$ term. Therefore, the $\sigma w(t/l)$ term is considered a constant offset to a linear fit of k versus $w(t/l)^3$. Figure 3(*e*) is the plot of the spring constant of the MoS_2 sheets versus $w(t/L)^3$ for seven different samples. The slope of the linear fit line suggests an E of 185 GPa. Using the offset of the linear fit, a pretension of 0.1 GPa was obtained. Besides this, all the seven measurements are bounded between $E = 185 \pm 50$ GPa and $\sigma = 0.1 \pm 0.02$ GPa.

We also investigated the thick MoS_2 beams. Figure 4(*d*) shows the indentation curve derived from three different spots on one beam whose thickness is about 45 nm, and the force curves demonstrate that for a thick MoS_2 beam the bending and stress terms in equation (4) are in dominant, so the beam is almost a linear system. The Young's modulus of about 170 GPa was deduced from the force curve of thick MoS_2 beams.

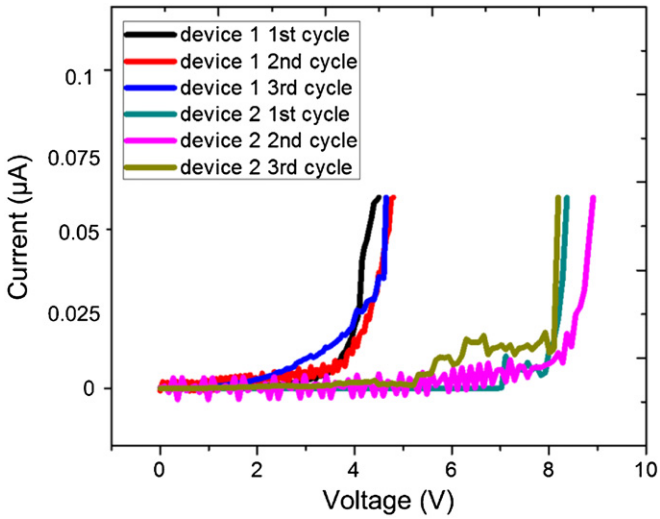

Figure 5. *I–V* measurement of two different MoS_2 switches. The pull-in voltages of the first switch are 4.5, 4.8, 4.6 V, respectively, and the pull-in voltages of the second switch are 8.4, 8.9, 8.2 V, respectively.

2.4. Investigation of the electrical properties of a MoS_2 MEMS switch

MoS_2 dc shunt MEMS switches are demonstrated. Once the applied dc bias is larger than the pull-in voltage of the switch, the top few-layer MoS_2 film is pulled down to be electrically in contact with the substrate, and a sharp increase in current is observed. The contact is broken by an elastic force after the bias is removed. The pull-in voltage of a MEMS switch is [37]:

$$V_{\mathrm{PI}} = \sqrt{\frac{8k_{\mathrm{eff}}g_0^3}{27\varepsilon A_{\mathrm{eff}}}} \tag{5}$$

where g_0 is the air gap between the suspended beam and substrate, ε is the vacuum permittivity, k_{eff} is the effective stiffness which includes the influence of pretension, and A_{eff} is the effective area. In our experiments the currents were measured as a function of dc bias voltage.

Figure 5 shows the measured *I–V* curves of two different few-layer MoS_2 switches (5 and 8 nm in thickness, respectively). The pull-in voltages of the first switch are 4.5, 4.8, 4.6 V, respectively, and the pull-in voltages of the second switch are 8.4, 8.9, 8.2 V, respectively, much smaller than the pull-in voltages of regular silicon MEMS switches [38, 39]. The three measured pull-in voltage values of each switch are very close, so they have good repeatability within the first few circles. We propose that the differences of V_{PI} for each switch are caused by two factors. First, the contact area/point and the air-gap height are not identical among switching. Second, the Joule heating during the switching can cause ambient molecular species to adsorb/desorb onto MoS_2 and modify the mechanical and surface properties of the MoS_2 beam.

3. Conclusion

In summary, we used an AFM pulsed force mode to compare the adhesion energy between MoS_2 and graphene, and observed that the adhesion energy of MoS_2 is smaller than graphene. Thus, in principle MEMS switches based on MoS_2 may have less stiction problems. Additionally, we observed that MoS_2 can be cleaned by O_2 plasma while etching graphene away rapidly. We fabricated suspended MoS_2 beam structures, and used an AFM to test the Young's modulus of the material. The Young's modulus of a few-layer MoS_2 is 185 GPa, and the Young's modulus of thick MoS_2 is 170 GPa. These are close to the values reported in [26, 27, 28]. We also characterized the suspended MoS_2 beams as MEMS switches. They have good repeatability within the first few cycles and their pull-in voltages are smaller than 10 V. The results presented here suggest that MoS_2 is a good candidate for MEMS switches.

Acknowledgment

The authors acknowledge the assistance of fabrication and characterization from Nanofabrication Center and the Characterization Facility at the University of Minnesota.

References

[1] Milaninia K M, Baldo M A, Reina A and Kong J 2009 All graphene electromechanical switch fabricated by chemical vapor deposition *Appl. Phys. Lett.* **95** 183105

[2] Li P, You Z, Haugstad G and Cui T 2011 Graphene fixed-end beam arrays based on mechanical exfoliation *Appl. Phys. Lett.* **98** 253105

[3] Sung M K, Song E B, Sejoon L, Sunae S, Seo D H, Yougha H, Candler R and Wang K L 2011 Suspended few-layer graphene beam electromechanical switch with abrupt on–off characteristics and minimal leakage current *Appl. Phys. Lett.* **99** 023103

[4] Duffy S, Bozler C, Rabe S, Knecht J, Travis L, Wyatt P, Keast C and Gouker M 2001 MEMS microswitches for reconfigurable microwave circuitry *IEEE. Microw. Wirel. Compon. Lett.* **11** 106–8

[5] Park J Y, Kim G H, Chung K W and Bu J U 2001 Monolithically integrated micromachined RF MEMS capacitive switches *Sensors Actuators* A **89** 88–94

[6] Goldsmith C L, Yao Z, Eshelman S and Denniston D 1998 Performance of low-loss RF MEMS capacitive switches *IEEE. Microw. Wirel. Compon. Lett.* **8** 269–71

[7] Hyman D and Mehregany M 1999 Contact physics of gold microcontacts for MEMS switches *IEEE. Trans. Compon. Packag. Technol.* **22** 357–64

[8] Hurst K M, Ansari N, Roberts C B and Ashurst W R 2011 Self-assembled monolayer-immobilized gold nanoparticles as durable, anti-stiction coatings for MEMS *J. Microelectromech. Syst.* **20** 424–35

[9] Novoselov K S, Geim A K, Morozov S V, Jiang D, Zhang Y, Dubonos S V, Grigorieva I V and Firsov A A 2004 Electric field effect in atomically thin carbon films *Science* **306** 666–9

[10] Geim A K 2009 Graphene: status and prospects *Science* **324** 1530–4

[11] Du X, Skachko I, Barker A and Andrei E Y 2008 Approaching ballistic transport in suspended graphene *Nature Nanotechnol.* **3** 491–5

[12] Lee C, Wei X, Kysar J W and Hone J 2008 Measurement of the elastic properties and intrinsic strength of monolayer graphene *Science* **321** 385–8

[13] Gomez-Navarro C, Burghard M and Kern K 2008 Elastic properties of chemically derived single graphene sheets *Nano Lett.* **8** 2045–49

[14] Frank I W, Tanenbaum D M, vander Zande A M and McEuen P L 2007 Mechanical properties of suspended graphene sheets *J. Vac. Sci. Technol.* B **25** 2558–61
[15] Koenig S P, Boddeti N G, Dunn M L and Bunch J S 2011 Ultrastrong adhesion of graphene membranes *Nature Nanotechnol.* **6** 543–6
[16] Bunch J S and Dunn M L 2012 Adhesion mechanics of graphene membranes *Solid State Commun.* **152** 1359–64
[17] Ma Y, Dai Y, Guo M, Niu C and Huang B 2011 Graphene adhesion on MoS_2 monolayer: an ab initio study *Nanoscale* **3** 3883–7
[18] Sen D, Novoselov K S, Reis P M and Buehler M J 2010 Tearing graphene sheets from adhesive substrates produces tapered nanoribbons *Small* **6** 1108–16
[19] Yoon T, Shin W C, Kim T Y, Mun J H, Kim T and Cho B J 2012 Direct measurement of adhesion energy of monolayer graphene as-grown on copper and its application to renewable transfer process *Nano Lett.* **12** 1448–52
[20] Li P, You Z and Cui T 2012 Graphene cantilever beams for nano switches *Appl. Phys. Lett.* **101** 093111
[21] Li P, You Z and Cui T 2012 Raman spectrum method for characterization of pull-in voltages of graphene capacitive shunt switches *Appl. Phys. Lett.* **101** 263103
[22] Shi Z *et al* 2012 Study of graphene-based nanoelectromechanical switches *Nano Res.* **5** 82–7
[23] Novoselov K S, Jiang D, Schedin F, Booth T J, Khotkevich W, Morozov S V and Geim A K 2005 Two-dimensional atomic crystals *Proc. Natl Acad. Sci. USA* **102** 10451–3
[24] Lee Y H *et al* 2012 Synthesis of large-area MoS_2 atomic layers with chemical vapor deposition *Adv. Mater.* **24** 2320–5
[25] Radisavljevic B, Radenovic A, Brivio J, Giacometti V and Kis A 2011 Single layer MoS_2 transistors *Nature Nanotechnol.* **6** 147–50
[26] Castellanos-Gomez A, Poot M, Steele G A, van der Zant H S J, Agrait N and Bollinger B R 2012 Elastic properties of freely suspended MoS_2, nanosheets *Adv. Mater.* **24** 772–5
[27] Castellanons-Gomez A, Poot M, Steele G A, van der Zant H S J, Agrait N and Rubio-Bollinger G 2012 Mechanical properties of freely suspended semiconducting graphene-like layers based on MoS_2 *Nanoscale Res. Lett.* **7** 1–4
[28] Bertolazzi S, Brivio J and Kis A 2011 Stretching and breaking of ultrathin MoS_2 *ACS Nano* **5** 9703–9
[29] Ong Y, Razatos A, Georgiou G and Sharma M M 1999 Adhesion forces between *E coli* bacteria and biomaterial surfaces *Langmuir* **15** 2719–25
[30] Burnham N A, Dominguez D D, Mowery R L and Colton R J 1990 Probing the surface forces of monolayer films with an atomic-force microscope *Phys. Rev. Lett.* **64** 1931–4
[31] Erts D, Lohmus A, Lohmus R, Olin H, Pokropivny A V, Ryen L and Svensson K 2002 Force interactions and adhesion of gold contacts using a combined atomic force microscope and transmission electron microscope *Appl. Surf. Sci.* **188** 460–6
[32] Maugis D 1992 Adhesion of spheres: the JKR-DMT transition using a dugdale model *J. Colloid. Interface Sci.* **150** 243–69
[33] Chidres I, Jauregui L A, Tian J and Chen Y P 2011 Effect of oxygen plasma etching on graphene studied using Raman spectroscopy and electronic transport measurements *New J. Phys.* **13** 025008
[34] Priessner M W, King T T, Kelly D P, Brover R, Calhoun L C and Ghodssi R 2003 Mechanical property measurement of InP- based MEMS for optical communications *Sensors Actuators* A **105** 190–200
[35] Lindahl N, Midtvedt D, Svensson J, Nerushev O A, Lindvall N, Isacsson A and Campbell E E B 2012 Determination of the bending rigidity of graphene via electrostatic actuation of buckled membranes *Nano Lett.* **12** 3526–31
[36] Senturia S D 2000 *Microsystem Design* (Boston, MA: Kluwer)
[37] Pamidighantam S, Puers R, Baert K and Tilmans H A 2002 Pull-in voltage analysis of electrostatically actuated beam structures with fixed-fixed and fixed-free end conditions *J. Micromech. Microeng.* **12** 458–64
[38] Nakatani T, Nguyen A T, Shimanouchi T, Imai M, Ueda S, Sawaki I and Satoh Y 2005 Single crystal silicon cantilever-based RF-MEMS switches using surface processing on SOI *18th IEEE Int. Conf. on Micro Electro Mechanical Systems (Miami Beach, FL, USA, 30 Jan.–3 Feb.)* pp 187–90
[39] Fruehling A, Pimpinella R, Nordin R and Peroulis D 2009 A single-crystal silicon DC-40 GHz RF MEMS switch *IEEE/MTT-S Int. Microwave Symp. (Boston, MA, USA, 7–12 June)* pp 1633–6